# First-principles investigations of the polysomatism of antigorite under pressure

**Jun Tsuchiya[1], Taiga Mizoguchi[1], Sayako Inoué[1], Elizabeth C. Thompson[2]**

[1]Geodynamics Research Center, Ehime University, 2-5 Bunkyo-cho, Matsuyama, Ehime 790-8577, JAPAN
[2]Department of Earth and Environmental Systems, The University of South, Sewanee, TN 37383, USA

**Key Points:**

- Antigorite crystal structures with various ($m$ = 14-19) were determined by first-principles calculation under pressure.
- The relative enthalpy shows that antigorite with smaller $m$-values are stabilized with increased pressure.
- Antigorite in suducting slabs may gradually dehydrate under high pressure as a result of changes to stable $m$-values.

Corresponding author: Jun Tsuchiya, junt@ehime-u.ac.jp

**Abstract**

Antigorite is the high-temperature member of the serpentine group minerals and is broadly considered a primary carrier of water in subducting oceanic lithosphere at the fore-arc. It has a wavy crystal structure along the $a$-axis and several polysomes with different $m$-values ($m$=13-24) have been identified in nature. The number ($m$) is defined as the number of tetrahedra in one wavelength and is controlled by the misfit between the octahedral and tetrahedral layers. The degree of misfit mainly depends on the volumes of the $MgO_6$ octehedra and $SiO_4$ tetrahedra within the layers, which vary as a function of temperature and pressure. However, it is not well understood which $m$-values of antigorite are stable at different temperature and pressure conditions. To investigate the pressure dependence of the stability of different $m$-values in antigorite, we performed first-principles calculations for several polysomes ($m$=14-19) at high pressure (0-14 GPa) and compared their enthalpies (T: static 0 K). We found that although the energy differences between polysomes are small, polysomes with larger $m$-values are more stable at ambient pressure, while polysomes with smaller $m$-values are more stable at elevated pressures. This suggests that the structure of antigorite in oceanic lithosphere that has subducted into the deep Earth may gradually evolve into a different polysome structure than antigorite samples observed at ambient or near-pressure conditions. This structural change may be related to the formation of the lower plane of the double seismic zone, as changes in polysome $m$-values are accompanied by a minor dehydration reaction.

## Plain Language Summary

Antigorite a hydrous mineral that is believe to be an important carrier for transporting water into the Earth's interior. However, its crystal structure is very complex, and is not well understood which structural variant is stable at the high temperature and pressure conditions of the Earth's interior. In this study, several crystal structures of antigorite were calculated by first-principles calculations, and their enthalpies were compared to determine the stable structure as a function of pressure. The results indicate that the structure and chemical composition of antigorite may change under high pressure, resulting in the gradual release of water. This behavior may explain the cause of deep focus earthquakes reported in the deep Earth.

## 1 Introduction

Serpentinite is a hydrous, ultramafic metamorphic rock composed of one or more of the serpentine subgroup minerals (antigorite, lizardite, chrysotile), and broadly considered the primary carrier of water in subducting oceanic lithosphere at forearcs. These serpentine subgroup minerals share the nominal formula $D_3[Si_2O_5](OH)_4$, in which D = Mg with minor substitution of Fe, Ni, Mn, Al, or Zn. These minerals are both common and hydrous, as they form by the hydrothermal metamorphism of mafic or ultramafic rocks in the oceanic lithosphere and mantle wedge through the process of serpentinization (Guillot & Hattori, 2013). Serpentinization also functions as a lubricant for subducting slabs, promoting aseismic slip due to the rheological weakness of serpentinite (Hilairet et al., 2007; Hirth & Guillot, 2007). Additionally, serpentinite is the primary carrier of water in subducting oceanic lithosphere and can transport water in a subducting cold plate to a depth of ∼200 km (e.g. Schmidt & Poli, 1998; Iwamori, 1998). Moreover, water released by the decomposition of serpentine minerals triggers magma generation in the mantle wedge above the subducting plate and is linked to island arc magmatism (Green, 2013; Tatsumi, 1986).

The stability and dehydration of serpentine minerals has also been extensively investigated in connection to intermediate and deep-focus earthquakes (e.g. (Peacock, 1990; Irifune et al., 1996; Omori et al., 2004; Komabayashi et al., 2005)). In particular, serpentine decomposition is thought to be closely related to the lower side of the Wadati-

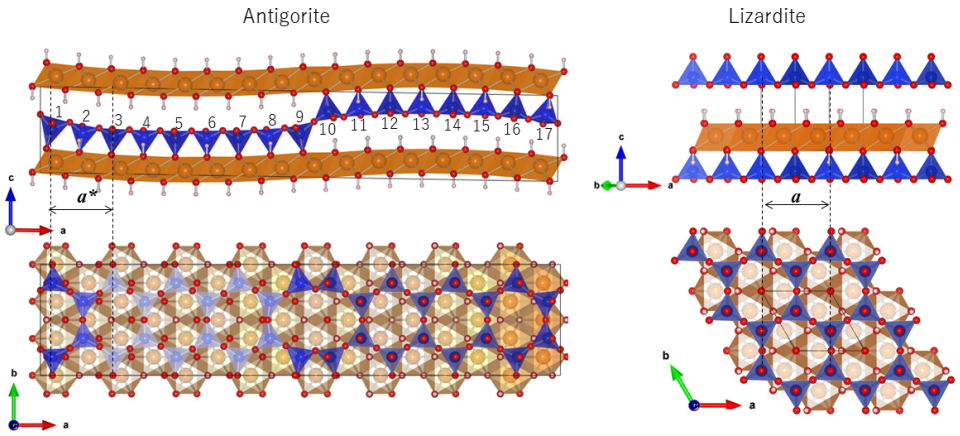


**Figure 1.** The structural differences between antigorite (m=17) and lizardite (m=$\infty$). $a^*$ corresponds to the averaged length of two $SiO_4$ tetrahedra along $a$-axis of antigorite.

Benioff zone (Nishiyama, 1992; Kirby et al., 1996; Yamasaki & Seno, 2003). However, the pressure-temperature ($P$–$T$) conditions under which such deep-focus earthquakes occur are not a perfect match for the phase boundaries of serpentine minerals as determined by laboratory experiments. Thus far, this discrepancy has been explained by the persistence of metastable serpentine in the subducting slab that eventually decomposes at sufficiently high $P$–$T$ conditions (Peacock, 1990). Since the formation and decomposition of serpentine minerals are intrinsically linked to a wide range of subduction zones dynamics, it is important to determine the depth to which these hydrous phases are stable, motivating experimental and theoretical studies that synthesize and/or evaluate serpentine minerals at variable pressure and temperature conditions.

All three serpentine minerals (lizardite, chrysotile, and antigorite) are phyllosilicates, with a 1:1 layer structure comprised of distinct layers of trioctahedral $Mg(O,OH)_6$ and tetrahedral $SiO_4$ polyhedra, which are more broadly described as $MO_6$ and $TO_4$ sheets, respectively. However, even at ambient $P$–$T$ conditions, there is a mismatch between the distance between the apical oxygen in the tetrahedral sheet (9.18 Å) and the oxygen-oxygen distance in the brucite-like octahedral sheet (9.44 Å) (Bailey, 1966). What differentiates the three serpentine minerals is how this ~3% discrepancy is resolved. In lizardite, which contains planar sheets of tetrahedral $TO_4$ and octahedral $MO_6$, the difference is resolved via Al-substitution in the octahedral layer and very small grain sizes (Mellini, 1982). In both chrysotile and antigorite, curvature is key, as the convex side of the $TO_4$ sheet contains stretched oxygen-oxygen distances which can then match the concave (i.e., compressed) side of an $MO_6$ sheet (Wicks & Whittaker, 1975). In chrysotile, the bending of the sheets is continuous, resulting in nanotubes that give the mineral a fibrous habit, whereas in antigorite the structure is alternating wavy or corrugated with layers interconnected and reversing the polarity of tetrahedral sheet at nodes along the $a$-axis (Figure 1) (Wicks & O'Hanley, 1988).

There are several structural variations of antigorite which are defined by the $m$-value that corresponds to the number of $TO_4$ tetrahedra within a single wavelength along the $a$-axis. Typically, the tetrahedra form six-membered rings, as in most phyllosilicates. However, the orientations of the tetrahedra are reversed at the nodes or points of inversion of the wavy structure where bending is most extreme, leading to structures referred to as "8-reversals" and "6-reversals" (Capitani & Mellini, 2005). In 8-reversals, the tetrahedra form the alternating 4- and 8-membered rings, where half of the convex of the tetrahedra are facing up and the other half are facing down. In 6-reversals, the tetrahedra form the 6-membered rings with four facing up and two facing down along the [010] direction. The 8-reversals and 6-reversals appear alternatively at the nodes of wavy structure along the $a$-axis. According to Kunze, 1961, the chemical formula of antigorite is described as $M_{3m-3}T_{2m}O_{5m}(OH)_{4m-6}$, where M is the octahedral site (M:$Mg^{2+}$, $Fe^{2+}$, $Al^{3+}$ etc.) and T is the tetrahedral sites (T: $Si^{4+}$, $Al^{3+}$, $Fe^{3+}$ etc.). In natural samples, $m = 13-24$ have been identified, corresponding to $C_{H2O} \simeq 12-12.5$ wt% (Mellini et al., 1987). Due to the link between polysomatism and chemical composition, antigorite is not a true polymorph of the other serpentine minerals, lizardite and chrysotile, due to its slight departure from the ideal $D_3[Si_2O_5](OH)_4$ formula.

HRTEM studies have shown that antigorite with an $m$-value of 17 is the most abundant phase, and many studies have focused exclusively on this crystal polysome (Capitani & Mellini, 2007). Indeed, most first-principles calculations have been performed using the $m = 17$ antigorite polysome structure (Mookherjee & Capitani, 2011; Capitani & Stixrude, 2012; Ghaderi et al., 2015; Demichelis et al., 2016; Balan et al., 2021). Despite this assumption, TEM studies of hydrothermally synthesized antigorites at various temperature and pressure conditions show that the $m$-value changes as a function of pressure and temperature (Wunder et al., 2001; Shen et al., 2020). Smaller $m$-value means an increase in the number of Si-O bonds bridging the layers per unit volume. This may cause an increase in attractive interaction between layers and thus an increase in density. Therefore, the phase diagram of antigorite which shows a decrease in $m$-value with increasing temperature is somewhat counter-intuitive. However, to date there has not been sufficient structural and thermodynamic corroboration regarding the stable polysome of antigorite at the $P$–$T$ conditions of a subducting oceanic plate.

Importantly, while lizardite and chrysotile are stable at low temperatures (Evans, 2004), antigorite only forms at elevated temperature (>250°C) and has the highest thermodynamic stability of the serpentine subgroup, increasing its importance as a host of hydrogen at increased depths. It has recently been suggested that polysomatism in the antigorite may be related to the reason why the deep seismicity at the lower surface of the Wadati-Benioff zone is not consistent with the phase boundary of the antigorite (Ferrant, 2019). As the temperature and pressure dependence of antigorite polysomatism, i.e., the $m$-value, has not been solved, this study uses first-principles calculations to: (1) determine structural models of antigorite with various $m$-values ($m$ = 14-19), and (2) calculate the pressure dependence of their relative enthalpies. This method allows us to investigate how the $m$-value, and therefore the chemical composition and dehydration, of antigorite varies as a function of pressure. The clarification of this behavior will make an important contribution to the understanding of the dehydration mechanism of serpentine in the deep Earth.

## 2 Methods

While density functional theory (DFT) (Hohenberg & Kohn, 1964; Kohn & Sham, 1965) is exact for the energy and density of the electronic ground state, in practice it is necessary to employ approximations to describe the many-body effects involved in the exchange-correlation functional. Possible approximations include a local density approximation (LDA) or a generalized gradient approximation (GGA). A hydrogen bond is an electrostatic force induced between a weakly positive hydrogen atom due to the forma-

tion of a covalent bond with a highly electronegative atom and a surrounding electronegative atom. Chemical interactions in phyllosilicates, including antigorites, are the result of subtle competition between covalent, hydrogen bonding, and van der Waals interactions. Describing the complexity of these interactions continues to be a very challenging task. The computational results for systems involving hydrogen bonding are sensitive to the choice of an appropriate exchange-correlation functional (e.g., Hamann, 1997), as the local-density approximations (LDA) tend to overestimate hydrogen bonding and generalized gradient approximations (GGA), while a significant improvement, do not account for long-range electron correlation forces. In this study, our first-principles calculations utilize a generalized gradient approximation with a Perdew-Burke-Ernzerhof functional (GGA-PBE) (Perdew et al., 1996), as it allows for direct comparison with previous ab initio calculations of hydrous minerals, especially the lizardite study of Tsuchiya, 2013.

The Troullier-Martins type norm-conserving pseudopotentials (Troullier & Martins, 1991), which were extensively tested in previous calculations (e.g., Tsuchiya and Tsuchiya 2008, 2009) were used for Mg, Si and H atoms. The ultrasoft pseudopotential for oxygen atom was generated by the method of Vanderbilt (Vanderbilt, 1990). The electronic wave function was expanded in plane waves using a kinetic energy cutoff of 50 Ry. The crystal structures of antigorite with $m = 16$ (space group $C2/m$) and 17 (space group $Pm$) have been reported (Capitani & Mellini, 2004, 2006) based on single crystal X-ray diffraction experiments. In this study, we generated and relaxed antigorite polysome structures ($m$=14-19), where the space groups of odd and even $m$ were set to $Pm$ and $C2/m$, respectively (Fig. 2) (Capitani & Mellini, 2005).

The irreducible Brillouin zone of the antigorite primitive cell were sampled on 2×2×2 ($m = 14, 16, 18$) and 1×3×3 ($m = 15, 17, 19$) Monkhorst-Pack meshes. This sampling is particularly important for the calculation of enthalpies of even and odd $m$ polysomes within comparable accuracy, as the primitive lattice vectors are totally different for the crystal structures of odd and even values of $m$ (Uehara & Shirozu, 1985). In addition to the calculation of antigorites, we also calculated the enthalpies of lizardite, forsterite ($Mg_2SiO_4$), brucite ($Mg(OH)_2$), phase A ($Mg_7Si_2O_8(OH)_6$), clinoenstatite ($MgSiO_3$), stishovite ($SiO_2$) and ice VIII ($H_2O$). The k-point samplings are summarized in Table 1. In order to estimate the dehydration pressure of antigorite, k-points samplings were conducted at 3×3×2 (phase A), 2×2×4 (clinoenstatite), 6×6×6 (ice-VIII) Monkhorst-Pack mesh. All structural parameters were fully relaxed at static 0 K using damped variable cell shape molecular dynamics using the quantum-espresso code (Giannozzi et al., 2009) until residual forces became less than $1.0\text{x}10^{-4}$ Ry/a.u.

In order to compare the enthalpies of antigorite with different $m$-values, the following chemical reactions were constructed with respect to lizardite:

$$Lizardite \leftrightarrow \frac{1}{m} Antigorite_m + \frac{3}{m} Brucite \tag{1}$$

$$Lizardite \leftrightarrow \frac{1}{m+3} Antigorite_m + \frac{6}{m+3} Forsterite + \frac{9}{m+3} IceVIII \tag{2}$$

Here $Antigorite_m$ indicates the chemical formula of antigorite with modulation of $m$ which is defined as $Mg_{3m-3}Si_{2m}\ O_{5m}(OH)_{4m-6}$. In this study, the enthalpy of ice VIII phase was used to investigate the dehydration reaction. This is because temperature effects are not considered in these calculations.

Since antigorite undergoes a phase transition to a dense hydrous magnesium silicate phase, phase A, under high pressure, the following chemical reaction was also calculated:

$$Lizardite \leftrightarrow \frac{1}{3} phaseA + \frac{2}{3} clinoenstatite + \frac{2}{3} stishovite + IceVIII \tag{3}$$

**Table 1.** The Monkhorst-Pack meshes and number of k points used in the calculation.

| Phase | k point mesh | number of k points |
|---|---|---|
| Antigorite ($m$:even) | 2×2×2 | 4 |
| Antigorite ($m$:odd) | 1×3×3 | 5 |
| Lizardite | 6×6×6 | 108 |
| Forsterite | 4×2×4 | 54 |
| Brucite | 6×6×4 | 72 |
| Phase A | 5×5×5 | 63 |
| Clinoenstatite | 4×4×4 | 32 |
| Stishovite | 4×4×6 | 9 |
| Ice VIII | 6×6×6 | 108 |

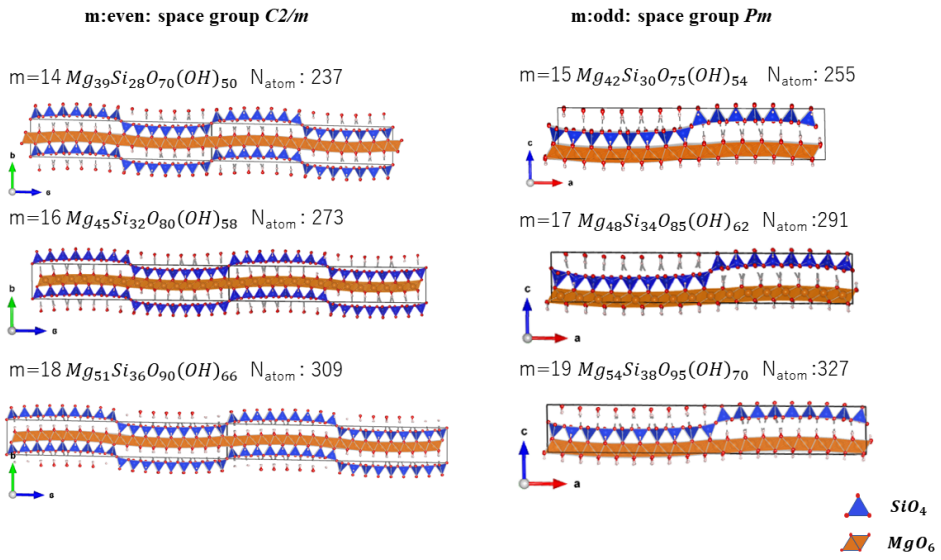


**Figure 2.** The model structures of antigorites ($m = 14 \sim 19$). The structures where $m$ is even indicate the primitive cell of the space group $C2/m$.

# 3 Results and Discussion

## 3.1 Structure optimization

*Antigorite*$_m$ has $m$ $SiO_4$ tetrahedra along the $a$-axis in the unit cell, while there are two $SiO_4$ tetrahedra along the $a$-axis in lizardite. Therefore, the $a$-axis of the antigorites were normalized to the length of two $SiO_4$ tetrahedra, the same as lizardite, and denoted as $a^*$ (Figure 1). The pressure variation of the lattice constants of antigorites are shown in Figure 3 and Table 2.

Calculated results indicate that the $a^*$ of antigorite is 3-5% shorter than that of lizardite, and this difference is more pronounced for antigorites with smaller $m$ (Figure 3A). This shrinkage is caused by pinning of the $m$ $SiO_4$ tetrahedra by the $m-1$ $MgO_6$ octahedra along the $a$-axis of antigorite. Without taking into account thermal expansion due to temperature effects, antigorites with smaller $m$-values are subject to more polyhedral distortion. Natural antigorites with $m$= 13-24 have been reported, and those with smaller $m$-values ($m$ <13) have not been found. This can be interpreted as the $SiO_4$ polyhedral distortion leads to structural instability of antigorites with small $m$-value.

There is little dependence on the $m$-value with respect to the change in the $b$ and $c$-axes of antigorite. As for lizardite, stable and metastable structures have been reported above approximately 8 GPa (Tsuchiya, 2013). No such metastable structures were found in antigorite. At low pressure, the length of the $c$-axis of antigorite is slightly smaller than that of lizardite, but above 8 GPa, the $c$-axis of the stable structure of lizardite is smaller. The higher $c$-axis compressibility of lizardite relative to that of antigorite has also been confirmed by experiments (Nestora et al., 2010; Hilairet et al., 2006). It was expected that as the $m$-value of antigorite decreases, the number of Si-O bonds connecting the layers per unit volume increases, causing an increase in density. However, contrary to this expectation, we found that the $m$-value dependence of the density of antigorite is almost negligible (Figure 3E, Table 2).

The high-pressure structure of $m = 17$ antigorite was reported based on the results of a single-crystal X-ray diffraction experiment (Nestora et al., 2010). The present calculations are in good agreement with these experiments within the accuracy of first-principles calculations based on GGA. GGA calculations typically result in volumes that are a few percent higher than experimental volumes due to slightly underestimated binding energies. The experiment of Nestola et al. (2010) reported softening of the antigorite lattice, especially the $c$-axis, and increase of the $\beta$ angle above 6 GPa. However, while softening was observed in the lizardite calculations, our antigorite calculations do not reveal softening when we evaluate the compressibility of the $c$-axis. Additionally, our antigorite calculations do not indicate an increase in the $\beta$-axis at pressures up to 14 GPa.

Overall, we find that within the antigorite lattice, the $b$-axis is less compressible than the $a$-axis. The $a$-axis of antigorite is also more compressible the $a$-axis of lizardite. These results are consistent with experiments and are tied to the wavy or corrugated structure of antigorite along the $a$-axis. We also observed that the compressibility of the $a$-axis is slightly higher for smaller $m$-value polysomes of antigorite. Both antigorite and lizardite contain hydrogen bonds along the $c$-axis which are weaker and therefore more easily compressed than other bonds. The $c$-axis compressibility of lizardite is higher than that of antigorite because the layers of lizardite are bound together only by hydrogen bonds, whereas antigorite also contains partial Si-O bonds between the layers. Somewhat surprisingly, however, the difference becomes more pronounced at higher pressures. Previous first-principles calculation of lizardite reported that the nature of hydrogen bonds in lizardite changes above 10 GPa (Tsuchiya, 2013), which may be responsible for the higher $c$-axis compressibility of lizardite, whereas the $c$-axis of antigorite is already compressed at low pressure and there is no commensurate shift in the nature of hydrogen bonds observed in antigorite at the pressures of this study (0-14 GPa).

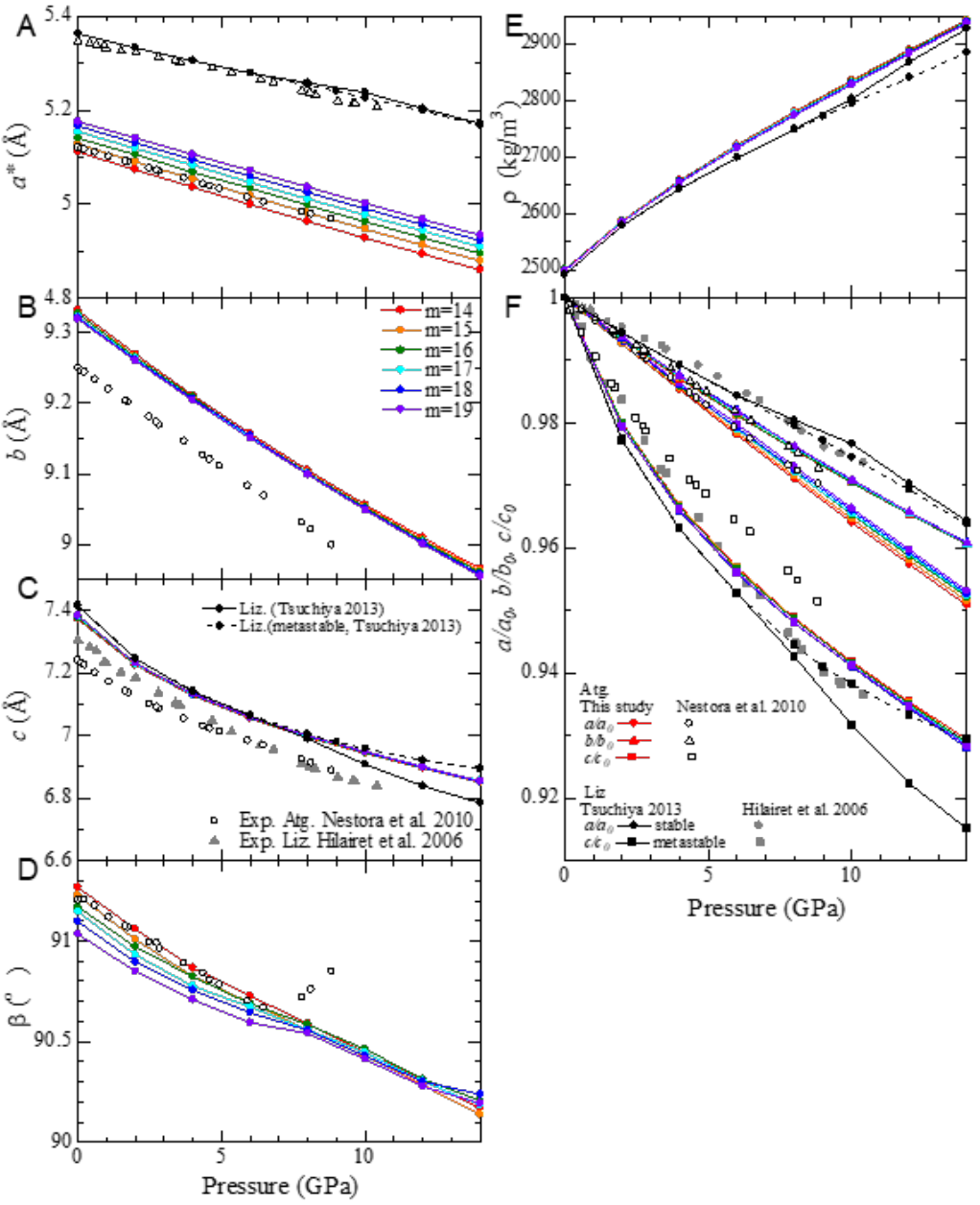


**Figure 3.** The full colored lines indicate the cell parameters (A∼D), density $\rho$ (E) and compressibilities (F) of antigorites ($m$ = 14-19). The $a^*$ corresponds to the two $SiO_4$ polyhedra along the $a$ lengths of $Antigorite_m$. Black full and dashed lines correspond to the stable and metastable cell lengths of lizardite (Tsuchiya, 2013), respectively. The black-open and full-gray symbols are previous single-crystal X-ray diffraction experiments of antigorite and lizardite, respectively (Nestora et al., 2010; Hilairet et al., 2006).

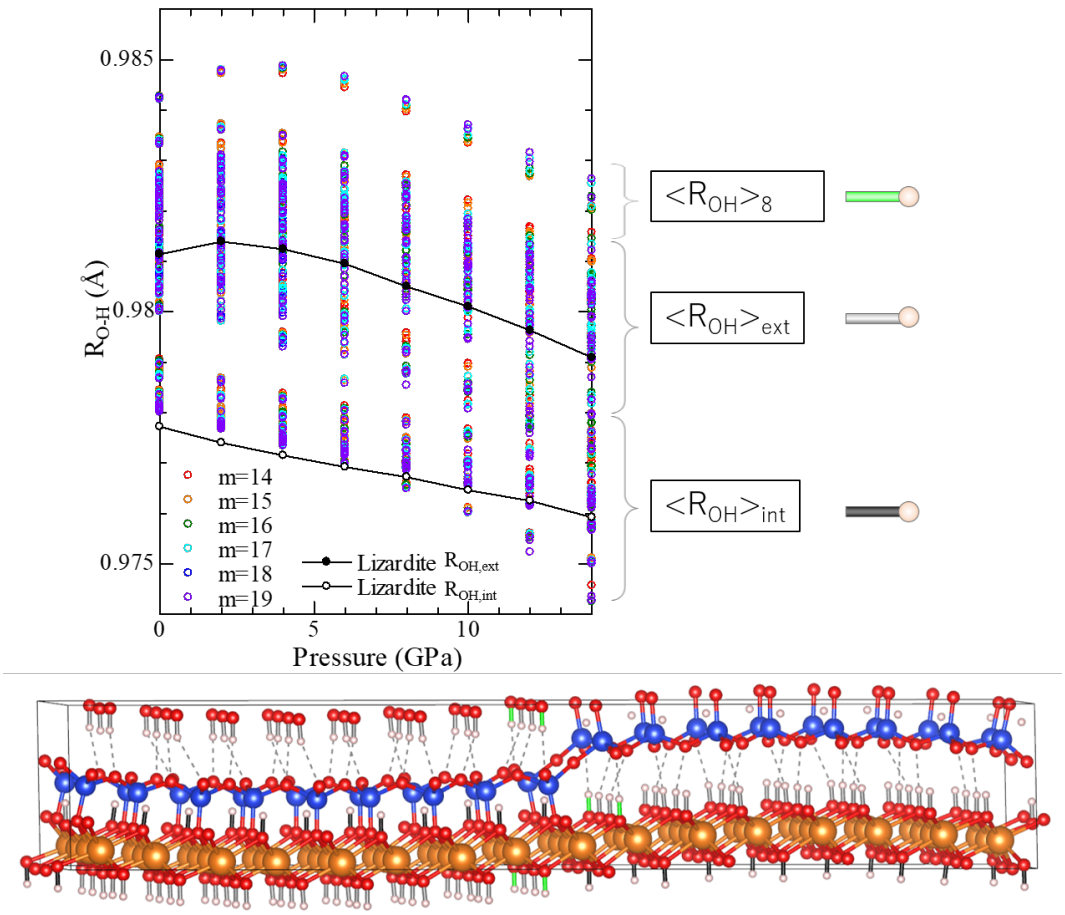


**Figure 4.** Pressure dependence of the OH distances of antigorites ($m$=14-19). $\langle R_{OH}\rangle_8$ indicates the OH distance oriented to the bridging oxygen atoms between the $SiO_4$ eight-membered rings (OH bond with green color) at 8-reversals. $\langle R_{OH}\rangle_{int}$ indicates the OH distance in the $SiO_4$ tetrahedral layers (black bond), and $\langle R_{OH}\rangle_{ext}$ indicates the OH distance oriented toward the interlayer voids (gray bond).

The pressure-dependence of the OH bond distances within the crystal structure of antigorite is shown in Figure 4. While lizardite has only two types of the OH bonds, one within the tetrahedral layers $R_{OH,int}$ and the other between the layers $R_{OH,ext}$, there are three main groups of OH covalent bonds, reflecting the complexity of antigorite's crystal structure. Two groups are similar to lizardite; one group of the OH bonds within the $SiO_4$ layer ($\langle R_{OH}\rangle_{int}$) and the other between layers ($\langle R_{OH}\rangle_{ext}$). The group unique to antigorite is the OH bonding group that forms hydrogen bonds to the bridging oxygen in the $SiO_4$ 4-membered rings existing at the 8-reversals ($\langle R_{OH}\rangle_8$). The OH bonds in that group have noticeably longer OH distances than the other two groups, suggesting that those hydrogen bonds are stronger. Due to the nature of the pseudopotentials used in this study, our results of the OH distances are longer than those of previous first-principles calculations conducted for $m$=17 antigorite, but the trend of OH distances at ambient pressure, $\langle R_{OH}\rangle_8 > \langle R_{OH}\rangle_{ext} > \langle R_{OH}\rangle_{int}$ is consistent (Balan et al., 2021). Although

**Table 2.** The calculated cell parameters and density ($\rho$) of antigorite ($m$ = 14-19).

| Pressure (GPa) | $a$ (Å) | $b$ (Å) | $c$ (Å) | $\beta$ (°) | $\rho$ (g/cm$^3$) |
|---|---|---|---|---|---|
| $m = 14$ | | | | | |
| 0 | 71.5529 | 9.3320 | 7.3727 | 91.267 | 2.4997 |
| 2 | 71.0224 | 9.2699 | 7.2252 | 91.059 | 2.5868 |
| 4 | 70.5033 | 9.2113 | 7.1277 | 90.867 | 2.6581 |
| 6 | 69.9822 | 9.1569 | 7.0546 | 90.728 | 2.7216 |
| 8 | 69.4775 | 9.1050 | 6.9948 | 90.589 | 2.7805 |
| 10 | 68.9803 | 9.0557 | 6.9435 | 90.445 | 2.8366 |
| 12 | 68.5050 | 9.0092 | 6.8962 | 90.309 | 2.8906 |
| 14 | 68.0333 | 8.9650 | 6.8521 | 90.169 | 2.9438 |
| $m = 15$ | | | | | |
| 0 | 38.4575 | 9.3281 | 7.3755 | 91.228 | 2.4994 |
| 2 | 38.1727 | 9.2663 | 7.2275 | 91.008 | 2.5866 |
| 4 | 37.9023 | 9.2084 | 7.1293 | 90.824 | 2.6574 |
| 6 | 37.6282 | 9.1537 | 7.0562 | 90.693 | 2.7205 |
| 8 | 37.3586 | 9.1020 | 6.9967 | 90.556 | 2.7791 |
| 10 | 37.0975 | 9.0528 | 6.9446 | 90.427 | 2.8349 |
| 12 | 36.8422 | 9.0061 | 6.8968 | 90.284 | 2.8892 |
| 14 | 36.5926 | 8.9615 | 6.8509 | 90.137 | 2.9429 |
| $m = 16$ | | | | | |
| 0 | 82.2465 | 9.3273 | 7.3770 | 91.171 | 2.4997 |
| 2 | 81.6855 | 9.2654 | 7.2284 | 90.971 | 2.5858 |
| 4 | 81.0803 | 9.2093 | 7.1298 | 90.823 | 2.6570 |
| 6 | 80.5381 | 9.1528 | 7.0564 | 90.688 | 2.7192 |
| 8 | 79.9587 | 9.1013 | 6.9972 | 90.584 | 2.7777 |
| 10 | 79.3946 | 9.0517 | 6.9456 | 90.462 | 2.8336 |
| 12 | 78.8472 | 9.0046 | 6.8976 | 90.313 | 2.8881 |
| 14 | 78.3113 | 8.9595 | 6.8525 | 90.206 | 2.9417 |
| $m = 17$ | | | | | |
| 0 | 43.8113 | 9.3231 | 7.3821 | 91.146 | 2.4984 |
| 2 | 43.5058 | 9.2635 | 7.2300 | 90.931 | 2.5852 |
| 4 | 43.2026 | 9.2062 | 7.1310 | 90.776 | 2.6558 |
| 6 | 42.8897 | 9.1523 | 7.0576 | 90.673 | 2.7189 |
| 8 | 42.5893 | 9.1002 | 6.9983 | 90.558 | 2.7770 |
| 10 | 42.2995 | 9.0500 | 6.9476 | 90.445 | 2.8320 |
| 12 | 42.0140 | 9.0022 | 6.9000 | 90.304 | 2.8862 |
| 14 | 41.7239 | 8.9569 | 6.8553 | 90.183 | 2.9399 |
| $m = 18$ | | | | | |
| 0 | 92.9955 | 9.3215 | 7.3833 | 91.096 | 2.4978 |
| 2 | 92.3451 | 9.2622 | 7.2309 | 90.895 | 2.5829 |
| 4 | 91.6948 | 9.2062 | 7.1317 | 90.756 | 2.6534 |
| 6 | 91.0616 | 9.1540 | 7.0572 | 90.643 | 2.7155 |
| 8 | 90.4388 | 9.0996 | 6.9989 | 90.557 | 2.7730 |
| 10 | 89.8244 | 9.0499 | 6.9477 | 90.428 | 2.8302 |
| 12 | 89.2063 | 9.0019 | 6.8983 | 90.301 | 2.8826 |
| 14 | 88.5949 | 8.9567 | 6.8522 | 90.238 | 2.9397 |
| $m = 19$ | | | | | |
| 0 | 49.1722 | 9.3196 | 7.3836 | 91.034 | 2.4984 |
| 2 | 48.8375 | 9.2606 | 7.2312 | 90.849 | 2.5847 |
| 4 | 48.5004 | 9.2037 | 7.1332 | 90.709 | 2.6546 |
| 6 | 48.1784 | 9.1502 | 7.0588 | 90.594 | 2.7163 |
| 8 | 47.8444 | 9.0985 | 6.9998 | 90.540 | 2.7739 |
| 10 | 47.5157 | 9.0483 | 6.9488 | 90.411 | 2.8292 |
| 12 | 47.1905 | 9.0001 | 6.9006 | 90.277 | 2.88439 |
| 14 | 46.8673 | 8.9541 | 6.8548 | 90.193 | 2.9382 |

there is a slight variation in the values, this trend is similar for all polysome structures of $m$=14-19.

The relationship between the strength of the hydrogen bond and the OH stretching vibration frequency has been investigated in a wide variety of materials, and it is generally believed that the stronger the hydrogen bond, the lower the OH stretching frequency. In the present study, some OH bonds in the 8-reversal are longer than other OH bonds, and the hydrogen bonds in the 8-reversal are considered stronger. First-principles calculations of the lattice vibrations of antigorite ($m$=17) under ambient pressure have been performed (Balan et al., 2021). The OH stretching vibration of antigorite has a broad asymmetric band of 3650-3750 $cm^{-1}$ at ambient pressure, and these OH bonds, which are unique to antigorite, have one of the lowest frequencies among them around 3650 $cm^{-1}$. This has been suggested to explain the weak and broad shoulder of the OH stretching band observed ∼3615 $cm^{-1}$ measured in the IR absorption band (Mellini et al., 2002).

No study has yet published direct, experimental measurements of the OH distances in antigorite under pressure. However, pressure variations in the OH stretching frequencies of lizardite, chrysotile, polygonal serpentine and antigorite have been reported using Raman spectroscopy (Auzende et al., 2004). The OH stretching vibrations attributed to $\langle R_{OH} \rangle_8$ have not yet been reported, but may explain the presence of experimentally determined low vibrational OH bands observed in antigorite at ∼3600 $cm^{-1}$, and which have either a negative pressure dependence or which are pressure independent. In previous dehydration experiments on antigorite, it has been reported that dehydration proceeds in two stages in the temperature range of 800-1000 K (Liu et al., 2019; Chollet et al., 2011). It is not difficult to speculate that antigorite dehydration may go through multiple stages with multiple bonding states as the ambient temperature structure contains three groups of OH bonds with different bond strengths.

### 3.2 Relative enthalpies

Figure 5(A) shows the pressure dependence of relative enthalpies for reactions (1) through (3). Reaction (1) is the change of lizardite to antigorite plus brucite. Since lizardite can be regarded as antigorite with $m = \infty$, the larger the number of $m$ of antigorite, the closer the enthalpy is to that of lizardite, and vice versa. Our results show that the enthalpy of the combination of antigorite ($m = 19$) and brucite is slightly lower than that of lizardite (about 0.2∼0.3 kJ/mol) between 0-5 GPa, but this is within the margin of error of the calculation and the phase stability cannot be evaluated based on such a marginal enthalpy difference. Since lizardite is reported to be the low-temperature phase of antigorite in nature, lizardite should essentially be the stable phase at static 0 K enthalpy. Similar enthalpy results have already been reported by an earlier study (Ghaderi et al., 2015, note that enthalpies in previous literature have been multiplied by $m$), with antigorite (+ brucite) being stabilized at ambient pressure using GGA, and lizardite appearing as the stable phase using LDA.

In the $Mg_3Si_2O_5(OH)_4$ composition, the stable phase changes from the combination of antigorite plus brucite to the combination of antigorite, forsterite plus $H_2O$ at about 5 GPa. The present calculations were performed at static 0 K, so ice VIII phase was used instead of liquid water, but this would correspond to a reaction that dehydrates above room temperature. Furthermore, at 7.2 GPa, the hydrous phase A (+ enstatite + stishovite + $H_2O$), known as the high-pressure hydrous phase of antigorite, has a lower enthalpy. This causes the stable region of antigorite to disappear.

The enthalpy values tend to increase with decreasing values of $m$ near ambient pressure. The enthalpy difference between $m = 19$ and 14 of antigorite at ambient pressure was about 1.3 kJ/mol. Antigorites with $m = 13-24$ have been identified in natural samples, and the absence of antigorites with $m$-values less than 13 may be due to

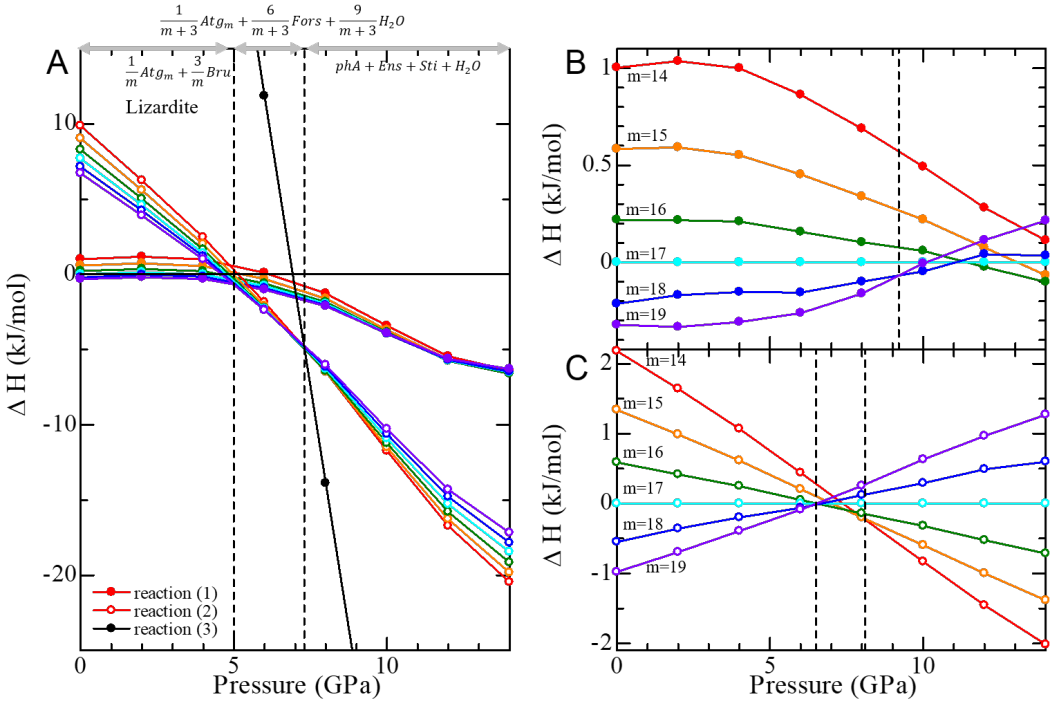


**Figure 5.** (A) The pressure dependence of the enthalpies of antigorite polysomes with different $m$-value ($m = 14 \sim 19$) with respect to lizardite ($m = \infty$). The colors in the legend are the same as in Figure 3. Relative enthalpy $\Delta H$ is the value of the right-hand side minus the left-hand side of reactions (1)-(3). (B) The ΔH of reaction (1) with respect to right side of reaction (1) for m=17, i.e., the enthalpy difference of reaction(1) in (A) rearranged with respect to that of m=17 line. (C) The ΔH of reaction (2) with respect to right side of reaction(2) for m=17, i.e., the enthalpy difference of reaction (2) in (A) rearranged with respect to that of m=17 line.

their higher enthalpies. On the other hand, no energetic evidence for the absence of antigorites with larger $m$ ($> 24$) was found from the present calculations.

The pressure dependence of the enthalpy of antigorite behaves differently depending on its $m$-value. In other words, at low pressure conditions, the larger the $m$ (i.e., $m$=19), the more stable the antigorite. On the other hand, at high pressure, the relationship between large and small values is reversed (Figure 5 BC). In Reaction (1), the enthalpy value crossing from $m$=19 to $m$=18 occurs at about 9.2 GPa, and at higher pressures, progressively smaller $m$ antigorites have lower enthalpies. This tendency is more pronounced in reaction (2), where the enthalpy value change from $m$ = 19 to 18 occurs at 6.5 GPa, and the lowest change to $m$ = 14 occurring at 8.1 GPa. Antigorite polysomes with $m$ = 19 and 14 have water contents of 12.4 wt% and 12.2 wt%, respectively. Although the difference in water content is slight, the change in $m$ from 19 to 14 requires that the antigorite releases water.

## 4 Geophysical implications

In this study, the $m$-dependence of antigorite under high pressure was investigated using first-principles calculations, and a comparison of the enthalpies of antigorite polysomes

with different $m$-values reveal that polysomes with smaller $m$-values are less stable at low pressure conditions, but become more stable relative to larger $m$-value polysomes at high pressures. This shift from larger to smaller $m$-value polysomes being stable occurs in a certain range of pressure. As shown in Figure 5C, the shift in $m$ from 19 to 14 occurs sequentially within a pressure range of about 1.6 GPa, from 6.5 GPa to 8.1 GPa. This change is accompanied by the release of a small amount of water (about 0.05 wt.%) as the $m$ of the antigorite decreases within this pressure range.

Wunder et al., 2001 pointed out that the $m$-frequency of antigorite may decrease under high temperature conditions. Komabayashi et al., 2005 also reported an $m$-value of 14 for antigorite synthesized at 2 GPa and 600°C, which is consistent with the results of Wunder et al., 2001. In this study, we did not calculate the free energy of antigorite at high temperatures using first-principles calculations, choosing to focus on relative stability at static 0 K due to limited computer resources. As a result, we found that the stable antigorite polysome structure changes with pressure. Taken together, these results suggest that the most frequent $m$-value of antigorite may decrease with pressure and temperature during the process of water transport to the Earth's deep interior through oceanic plate subduction. Thus, the dehydration of antigorite would not occur at a single discrete pressure and temperature, but rather the boundary is expected to have a fixed width related to the sequential polysomatism from large to small $m$-value polysomes.

In this study, calculations are performed only on pure Mg,Si-antigorites and the effects of impurities, especially Al and Fe, are ignored. As mentioned in the introduction, the structure of antigorite is controlled by the misfit between M and T sheets. Therefore, it is highly possible that impurities in these sheets can change the amount of misfit between the sheets and influence the stable polysome of antigorite at a given pressure and temperature. Additionally, as reported based on electron microscopy observations, the enthalpy differences between antigorites with different $m$-values are so small that antigorites with multiple $m$-values coexist metastably under finite temperature conditions. The results of our enthalpy calculations indicate that the $m$-value of the most frequent polysomes varies with pressure, but it is likely that multiple polysomes coexist in each state.

The physical mechanisms of intermediate-depth and deep-focus earthquakes, which occur at $P$–$T$ conditions that should produce ductile deformation rather than brittle fracture, have been debated because the triggering mechanisms are unexplained. The most commonly cited link to intermediate-depth earthquake activity is dehydration embrittlement. However, laboratory experiments on dehydration embrittlement do not explain all the characteristics of these earthquakes. In particular, the cause of the lower plane of the Wadati-Benioff double seismic zone has yet to be elucidated (Kita & Ferrand, 2018). It may be important to consider the phase boundary and dehydration of antigorite will have a width when discussing the region where deep-focus earthquakes occur. This study points out the possibility that the structure and chemical composition of antigorite in the Earth's interior may differ from that at the Earth's surface. Changes in the chemical composition of antigorite are likely to alter its thermodynamic stability fields. Additional experiments and theoretical calculations are needed to investigate the relationship between the breadth of antigorite stability region and the lower Wadati-Benioff zone.

## 5 Conclusions

In this study, first-principles calculations were performed for different polysomes ($m$=14-19) of antigorite to determine the crystal structure and enthalpy at 0-14 GPa and 0 K. In the pressure range up to 0-6 GPa, polysomes with larger $m$ ($m$=19) antigorite polysomes were found to be stable, while structures with smaller $m$ ($m$=14) were found to be stable under high pressure above 8 GPa. The $m$-value of stable antigorite changes gradually in the pressure range in between. Each of these changes is accompanied by slight

dehydration. Therefore, the dehydration reaction of antigorite under pressure does not occur all at once at the phase boundary, but may proceed stepwise with the $m$ change over a certain pressure range. Such phenomena should be taken into account in studying the relationship between dehydration and dynamic phenomena in serpentine transported into the Earth's interior. It is necessary to quantitatively evaluate the dehydration of these phenomena at high temperatures and to investigate the effects of impurities such as iron and aluminum in the future.

**Acknowledgments**

This work was supported by JSPS KAKENHI Grant Number JP20K04043, JP20K04126 and JP23H01273. The computation was carried out using the General Projects on supercomputer "Flow" at Information Technology Center, Nagoya University.

## References

Auzende, A.-L., Daniel, I., Raynard, B., Lemaire, C., & Guyot, F. (2004). High-pressure behaviour of serpentine minerals: A Raman spectroscopic study. *Phys. Chem. Minerals*, *31*, 269-277. doi: 10.1007/s00269-004-0384-0

Bailey, S. W. (1966). The status of clay mineral steuctures. *Clays Clay Miner.*, *14*, 1–823. doi: 10.1346/CCMN.1966.014010

Balan, E., Fritsch, E., Radtke, G., Paulatto, L., Juillot, F., & Petit, S. (2021). First-principles modeling of the infrared spectrum of antigorite. *European Journal of Mineralogy*, *33*, 389–400. doi: 10.5194/ejm-33-389-2021

Capitani, G. C., & Mellini, M. (2004). The modulated crystal structure of antigorite: The m = 17 polysome. *Am. Mineral.*, *89*, 147–158.

Capitani, G. C., & Mellini, M. (2005). HRTEM evidence for 8-reversals in the m = 17 antigorite polysome. *Am. Mineral.*, *90*, 991–999. doi: 10.2138/am.2005.1634

Capitani, G. C., & Mellini, M. (2006). The crystal structure of a second antigorite polysome (m=16), by single-crystal synchrotron diffraction. *Am. Mineral.*, *91*, 394–399. doi: doi:10.2138/am.2006.1919

Capitani, G. C., & Mellini, M. (2007). High-resolution transmission electron microscopy (HRTEM) investigation of antigorite polysomes ($m$ = 15 to 18). *Am. Mineral.*, *92*, 64–71. doi: 10.2138/am.2007.2188

Capitani, G. C., & Stixrude, L. (2012). A first-principle investigation of antigorite up to 30 GPa: Structural behavior under compression. *Am. Mineral.*, *97*, 1177–1186. doi: 10.2138/am.2012.3956

Chollet, M., Daniel, I., Koga, K. T., Morard, G., & van de Moortèle, B. (2011). Kinetics and mechanism of antigorite dehydration: Implications for subduction zone seismicity. *J. Geophys. Res.*, *116*, B04203. doi: 10.1029/2010JB007739

Demichelis, R., De La Pierre, M., Mookherjee, M., Zicovich-Wilson, C. M., & Orlandod, R. (2016). Serpentine polymorphism: A quantitative insight from first-principles calculations. *Cryst. Eng. Comm.*, *18*, 4412—4419. doi: 10.1039/c6ce00190d

Evans, B. W. (2004). The serpentinite multisystem revisited: Chrysotile is metastable. *International Geology Review*, *46*, 479–506. doi: 10.2747/0020-6814.46.6.479

Ferrant, T. (2019). Neither antigorite nor its dehydration is "metastable". *Am. Mineral.*, *104*, 788-–790. doi: 10.2138/am-2019-6957

Ghaderi, N., Zhang, H., & Sun, T. (2015). Relative stability and contrasting elastic properties of serpentine polymorphs from first-principles calculations. *J. Geophys. Res. Solid Earth*, *120*, 4831–4842. doi: 10.1002/2015JB012148

Giannozzi, P., Baroni, S., Bonini, N., Calandra, M., Car, R., Cavazzoni, C., ... Wentzcovitch, R. M. (2009). QUANTUM ESPRESSO: a modular and open-

source software project for quantum simulations of materials. *J. Phys.: Condens. Matter*, *21*, 395502. doi: 10.1088/0953-8984/21/39/395502

Green, H. W., II. (2013). Shearing instabilities accompanying high-pressure phase transformations and the mechanics of deep earthquakes. *Proceedings of the National Academy of Sciences*, *104*, 107-113. doi: 10.1073/pnas.0608045104

Guillot, S., & Hattori, K. (2013). Serpentinites: Essential roles in geodynamics, arc volcanism, sustainable development, and the origin of life. *Elements*, *9*, 95-98. doi: 10.2113/gselements.9.2.95

Hamann, D. (1997). $H_2O$ hydrogen bonding in density-functional theory. *Phys. Rev. B*, *55*, R10157.

Hilairet, N., Daniel, I., & Reynard, B. (2006). P–V equations of state and the relative stabilities of serpentine varieties. *Phys. Chem. Minerals*, *33*, 629–639. doi: 10.1007/s00269-006-0111-0

Hilairet, N., Reynard, B., Wang, Y., Daniel, I., Merkel, S., Nishiyama, N., & Petitgirard, S. (2007). High-pressure creep of serpentine, interseismic deformation, and initiation of subduction. *Science*, *318*, 1910–1913. doi: 10.1126/science.1148494

Hirth, G., & Guillot, S. (2007). Rheology and tectonic significance of serpentinite. *Elements*, *9*, 9133-9138. doi: 10.2113/gselements.9.2.107

Hohenberg, P., & Kohn, W. (1964). Inhomogeneous electron gas. *Phys. Rev.*, *136*, B864-B871.

Irifune, T., Kuroda, K., Funamori, N., Uchida, T., Yagi, T., Inoue, T., & Miyajima, N. (1996). Amorphization of serpentine at high pressure and high temperature. *Science*, *272*, 1468–1470.

Iwamori, H. (1998). Transportation of $H_2O$ and melting in subduction zones. *Earth Planet. Sci. Lett.*, *160*, 65–80.

Kirby, S., Engdahl, R. E., & Denlinger, R. (1996). *Intermediate-depth intraslab earthquakes and arc volcanism as physical expressions of crustal and uppermost mantle metamorphism in subducting slabs* (G. Bebout, D. W. School, S. H. Kirby, & J. P. Platt, Eds.). Washington, DC, USA: Geophysical Monograph Series (American Geophysical Union).

Kita, S., & Ferrand, T. (2018). Physical mechanisms of oceanic mantle earthquakes: Comparison of natural and experimental events. *Sci. Rep.*, *8*, 17049. doi: 10.1038/s41598-018-35290-x

Kohn, W., & Sham, L. (1965). Self-consistent equations including exchange and correlation effects. *Phys. Rev.*, *140*, A1133-A1138.

Komabayashi, T., Hirose, K., Funakoshi, K., & Takafuji, N. (2005). Stability of phase A in antigorite (serpentine) composition determined by in situ X-ray pressure observations. *Phys. Earth Planet. Inter.*, *151*, 276–289. doi: 10.1016/j.pepi.2005.04.002

Kunze, G. (1961). Antigorit. strukturtheoretische grundlagen und ihre praktische bedeutung fur die weitere serpentin-forschung. *Fortshr. Mineral.*, *39*, 206–324.

Liu, T., Wang, D., Shen, K., Liu, C., & Yi, L. (2019). Kinetics of antigorite dehydration: Rapid dehydration as a trigger for lower-plane seismicity in subduction zones. *Am. Mineral*, *104*, 282-290. doi: 10.2138/am-2019-6805

Mellini, M. (1982, 01). The crystal structure of lizardite 1t: Hydrogen bonds and polytypism. *American Mineralogist*, *67*, 587-598.

Mellini, M., Fuchs, Y., Viti, C., Lemaire, C., & Linarés, J. (2002). Insights into the antigorite structure from Mössbauer and FTIR spectroscopies. *European Journal of Mineralogy*, *14*, 97–104. doi: 10.1127/0935-1221/2002/0014-0097

Mellini, M., Trommsdorff, V., & Capitani, G. C. (1987). Antiforite polysomatism: Behavior during progressive metamorphism. *Contrib. Mineral Petrol.*, *97*, 147–155. doi: 10.1007/BF00371235

Mookherjee, M., & Capitani, G. C. (2011). Trench parallel anisotropy and large delay times: Elasticity and anisotropy of antigorite at high pressures. *Geophys.*

*Res. Lett.*, *38*, L09315. doi: 10.1029/2011GL047160

Nestora, F., Angel, R. J., Zhao, J., Garrido, C. J., Sánchez-Vizcaíno, V. L., Capitani, G., & Mellini, M. (2010). Antigorite equation of state and anomalous softening at 6 GPa: An in situ single-crystal x-ray diffraction study. *Contrib. Mineral. Petrol.*, *160*, 33–43. doi: 10.1007/s00410-009-0463-9

Nishiyama, T. (1992). Mantle hydrology in a subduction zone: A key to episodic geologic events, double Wadati-Benioff zones and magma genesis. Mathematical Seismology, VII. *Report of The Institute of Statistical Mathematics, Tokyo*, *34*, 31–67.

Omori, S., Komabayashi, T., & Maruyama, S. (2004). Dehydration and earthquakes in the subducting slab: Empirical link in intermediate and deep seismic zones. *Phys. Earth Planet. Inter.*, *146*, 297–311. doi: 10.1016/j.pepi.2003.08.014

Peacock, S. M. (1990). Are the lower planes of double seismic zones caused by serpentine dehydration in subducting oceanic mantle? *Geology*, *29*, 299–302.

Perdew, J. P., Burke, K., & Ernzerhof, M. (1996). Generalized gradient approximation made simple. *Phys. Rev. Lett.*, *77*, 3865–3868. doi: 0.1103/PhysRevLett .77.3865.

Schmidt, M. W., & Poli, S. (1998). Experimentally based water budgets for dehydrating slabs and consequences for arc magma generation. *Earth Planet. Sci. Lett.*, *163*, 361-379. doi: 10.1016/S0012-821X(98)00142-3

Shen, T., Zhang, C., Chen, J., Hermann, J., Zhang, L., Padrón-Navarta, J. A., ... Yang, J. (2020). Changes in the cell parameters of antigorite close to its dehydration reaction at subduction zone conditions. *Am. Mineral*, *105*, 569–582. doi: 10.2138/am-2020-7159

Tatsumi, Y. (1986). Formation of the volcanic front in subduction zones. *Geophysical Research Letters*, *13*(8), 717-720. doi: 10.1029/GL013i008p00717

Troullier, N., & Martins, J. (1991). Efficient pseudopotential for plane wave calculations. *Phys. Rev. B.*, *43*, 1993-2006.

Tsuchiya, J. (2013). A first-principles calculation of the elastic and vibrational anomalies of lizardite under pressure. *Am. Mineral.*, *98*, 2046–2052.

Uehara, S., & Shirozu, H. (1985). Variations in chemical composition and structural properties of antigorites. *Mineral. J.*, *12*(7), 299-318. doi: 10.2465/minerj.12 .299

Vanderbilt, D. (1990). Soft self-consistent pseudopotentials in a generalized eigenvalue formalism. *Phys. Rev. B*, *268*, 858–861. doi: 10.1103/PhysRevB.41 .7892

Wicks, F. J., & O'Hanley, D. S. (1988). Serpentines: Structures and Petrology. In S. W. Bailey (Ed.), *Hydrous phyllosilicates exclusive of micas* (Vol. 19, p. 91-168). Mineralogical Society of America.

Wicks, F. J., & Whittaker, E. J. W. (1975). A reappraisal of the structures of the serpentine minerals. *The Canadian Mineralogist*, *13*(3), 227-243.

Wunder, B., Wirth, R., & Gottscharlk, M. (2001). Antigorite: Pressure and temperature dependence of polysomatism and water content. *Eur. J. Mineral.*, *113*, 485–495. doi: 10.1127/0935-1221/2001/0013-0485

Yamasaki, T., & Seno, T. (2003). Double seismic zone and dehydration embrittlement of the subducting slab. *J. Geophys. Res. Solid Earth*, *108*, 2212. doi: 10 .1029/2002JB001918

**Figure 1.**

Antigorite

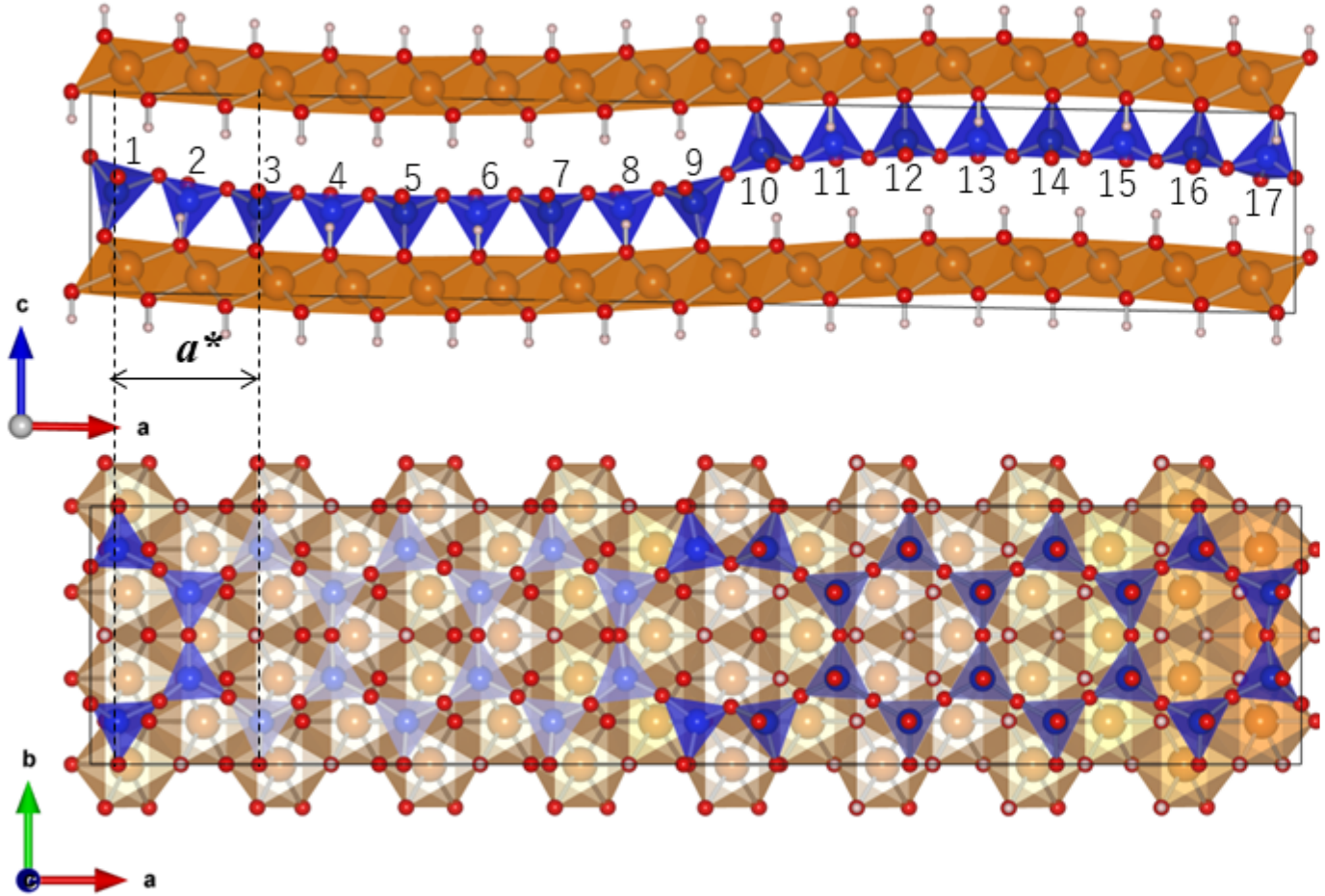


Lizardite

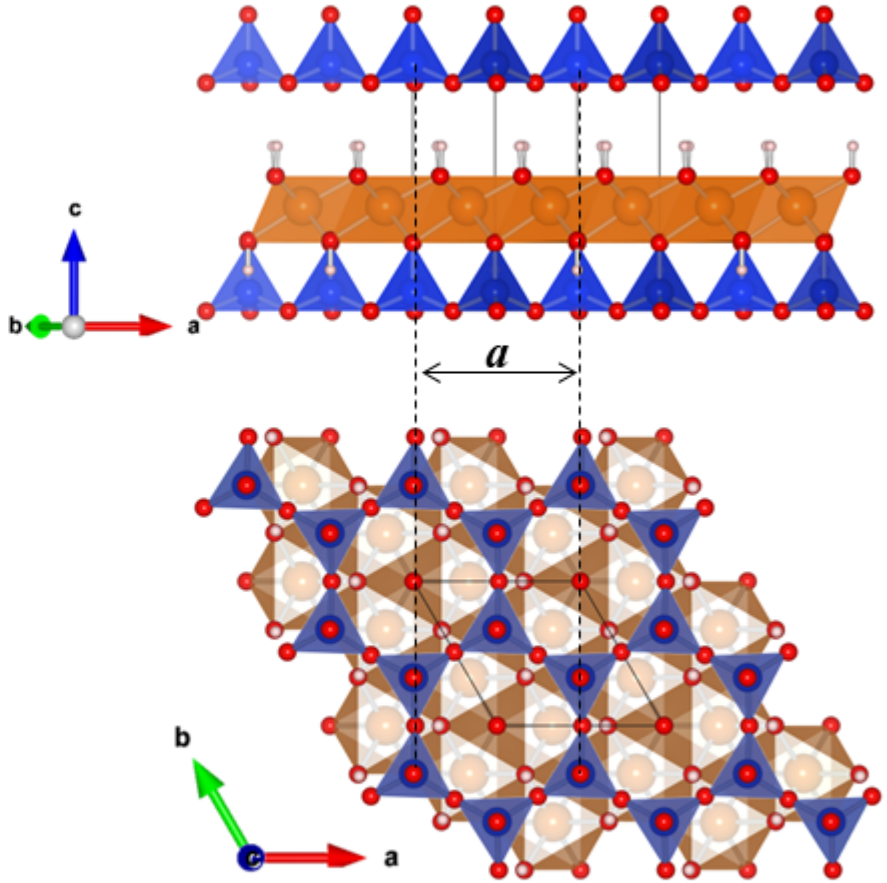

**Figure 2.**

**m:even: space group *C2/m***

m=14 $Mg_{39}Si_{28}O_{70}(OH)_{50}$ $N_{atom}$ : 237

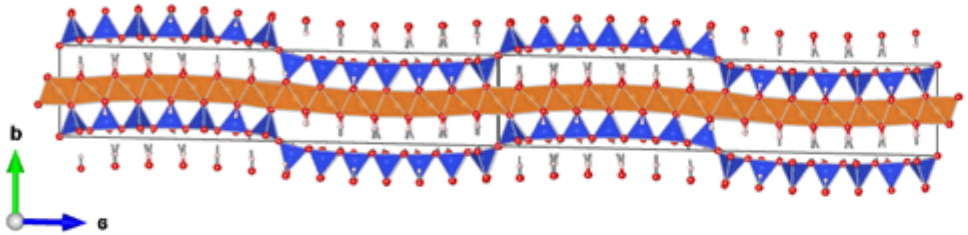


m=16 $Mg_{45}Si_{32}O_{80}(OH)_{58}$ $N_{atom}$ : 273

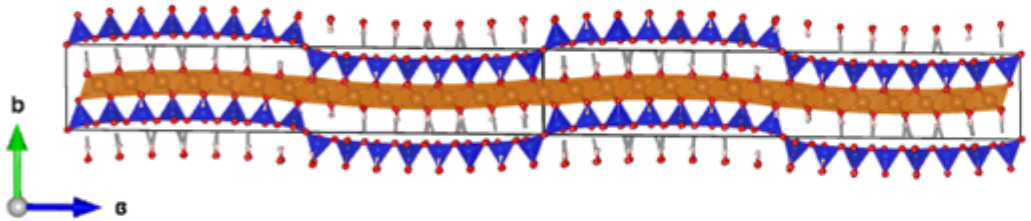


m=18 $Mg_{51}Si_{36}O_{90}(OH)_{66}$ $N_{atom}$ : 309

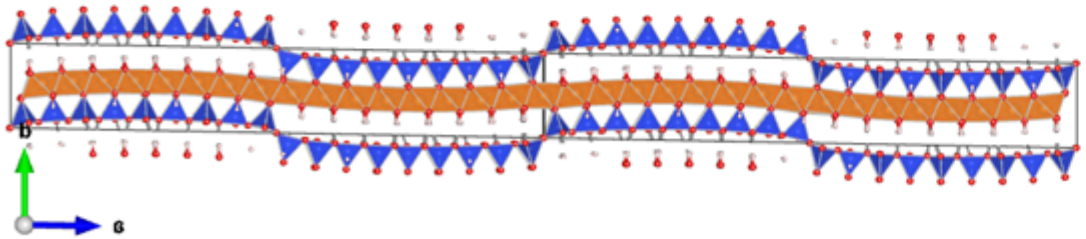


**m:odd: space group *Pm***

m=15 $Mg_{42}Si_{30}O_{75}(OH)_{54}$ $N_{atom}$: 255

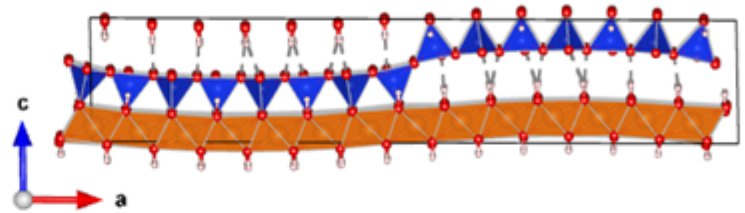


m=17 $Mg_{48}Si_{34}O_{85}(OH)_{62}$ $N_{atom}$ :291

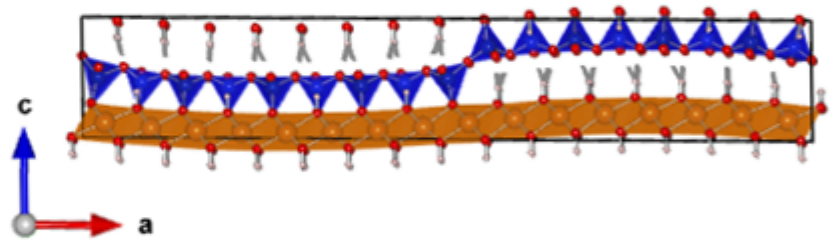


m=19 $Mg_{54}Si_{38}O_{95}(OH)_{70}$ $N_{atom}$ :327

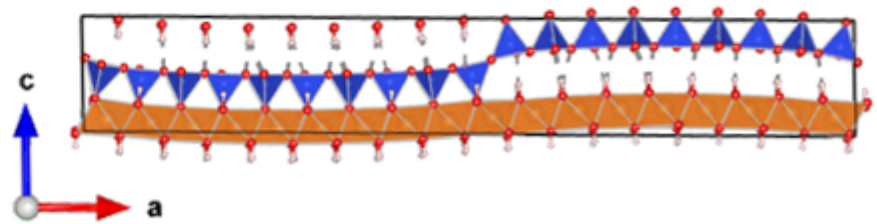


**Figure 3.**

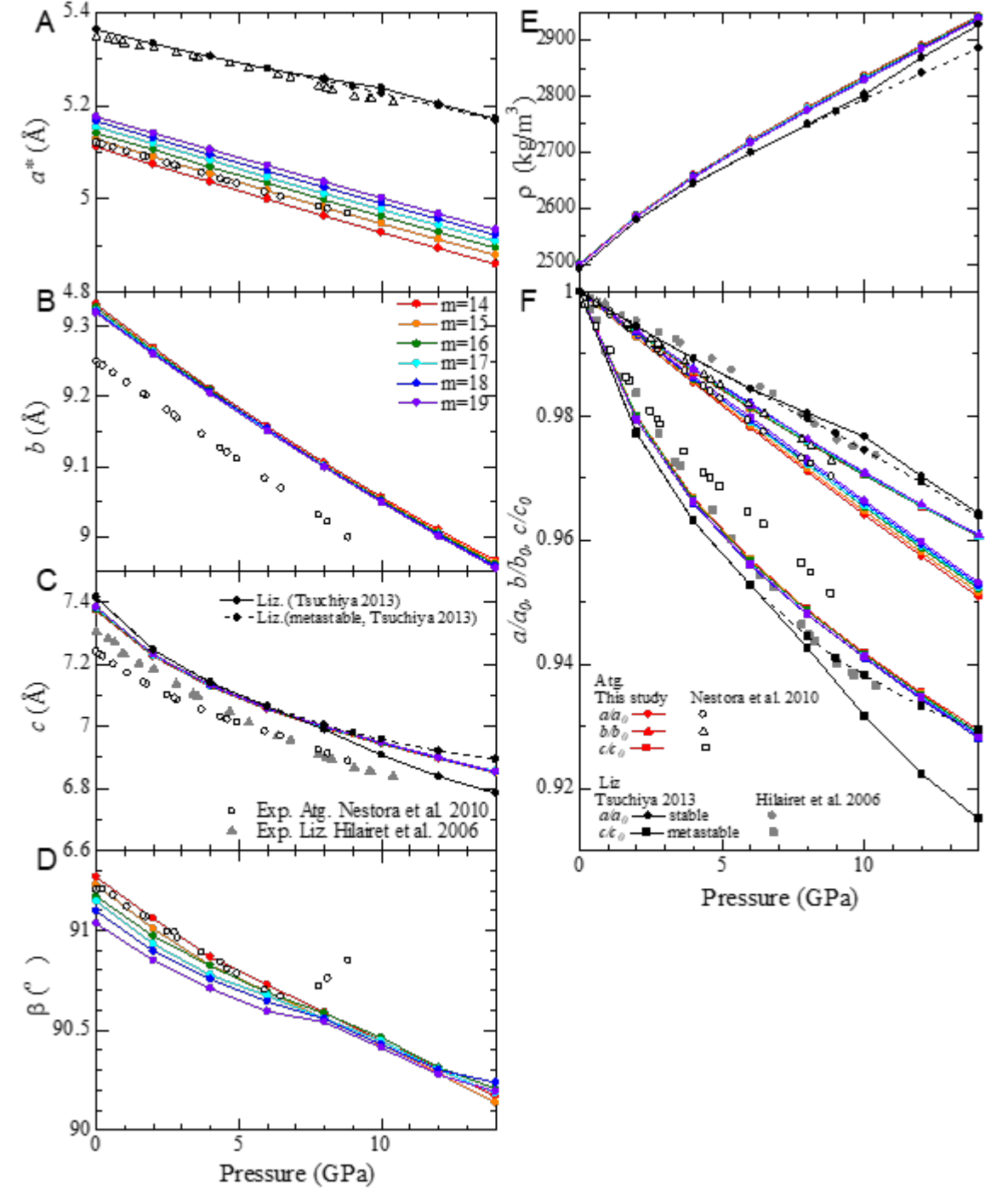
A
B
C
D
E
F
a* (Å)
b (Å)
c (Å)
β (°)
ρ (kg/m3)
a/a0, b/b0, c/c0
m=14
m=15
m=16
m=17
m=18
m=19
Liz. (Tsuchiya 2013)
Liz.(metastable, Tsuchiya 2013)
Exp. Atg. Nestora et al. 2010
Exp. Liz. Hilairet et al. 2006
Atg.
This study
Nestora et al. 2010
Liz
Tsuchiya 2013
stable
metastable
Hilairet et al. 2006
Pressure (GPa)
Pressure (GPa)

**Figure 4.**

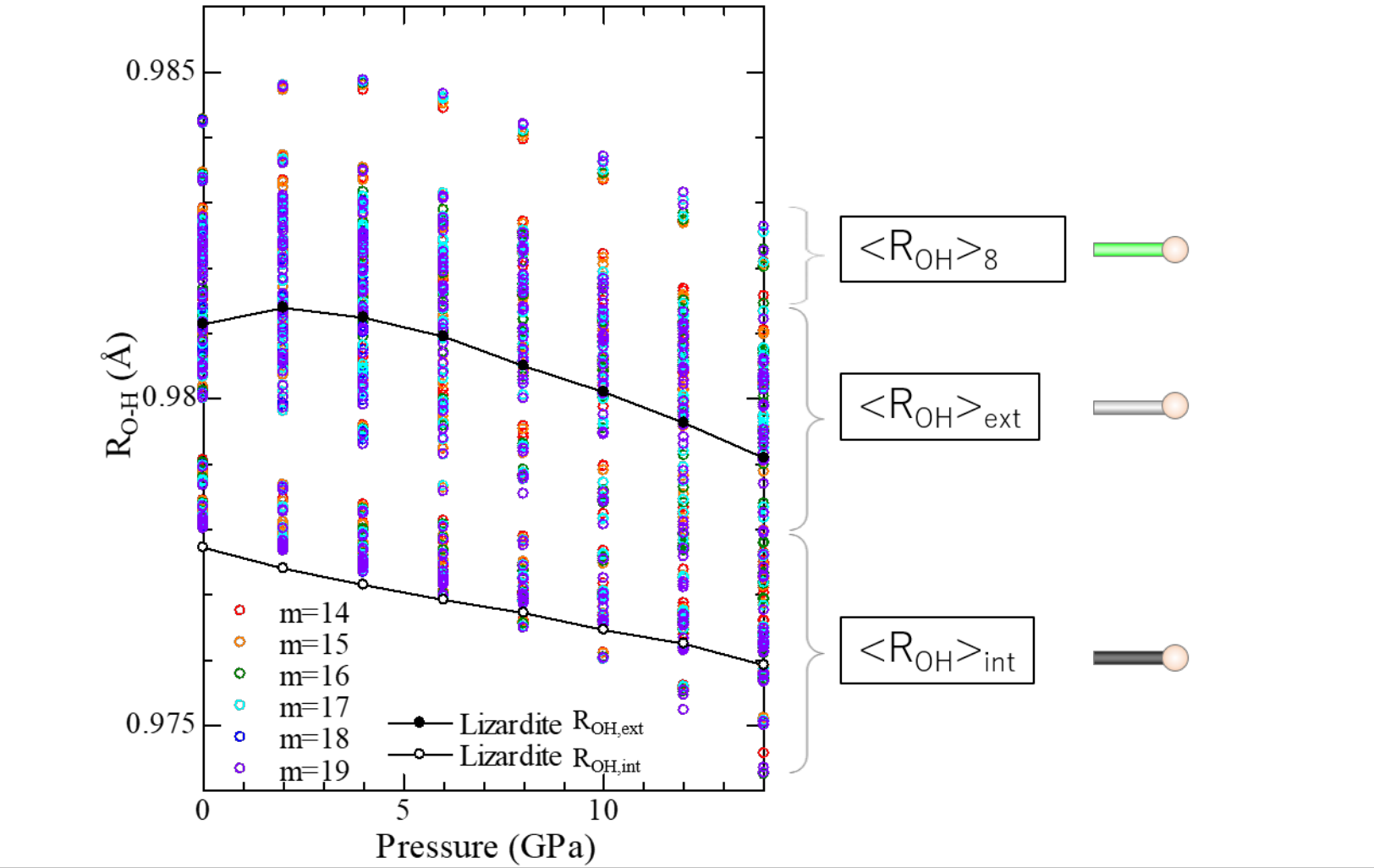
0.985
0.98
0.975
$R_{O-H}$ (Å)
0
5
10
Pressure (GPa)
m=14
m=15
m=16
m=17
m=18
m=19
Lizardite $R_{OH,ext}$
Lizardite $R_{OH,int}$
$<R_{OH}>_8$
$<R_{OH}>_{ext}$
$<R_{OH}>_{int}$

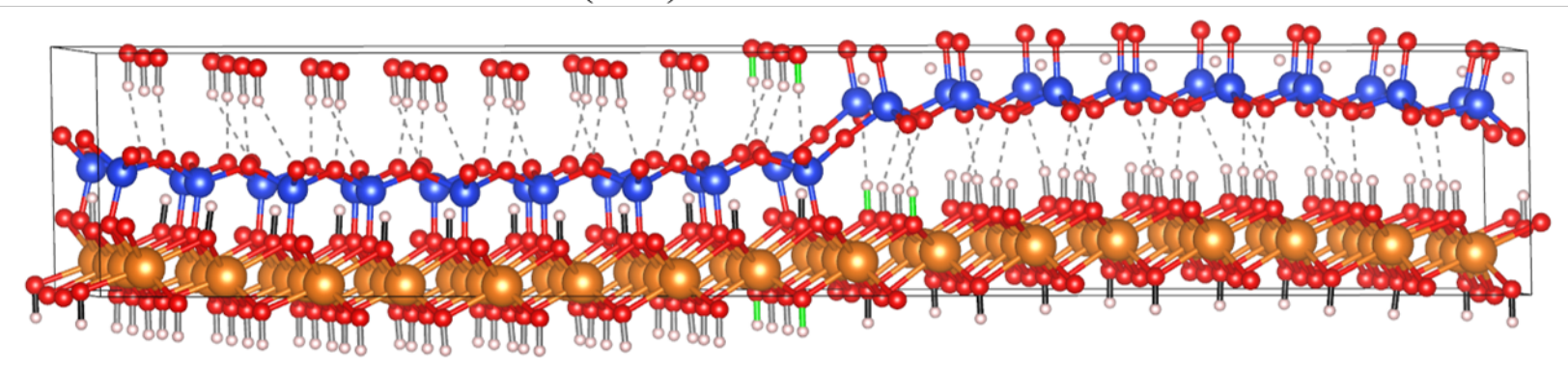

**Figure 5.**

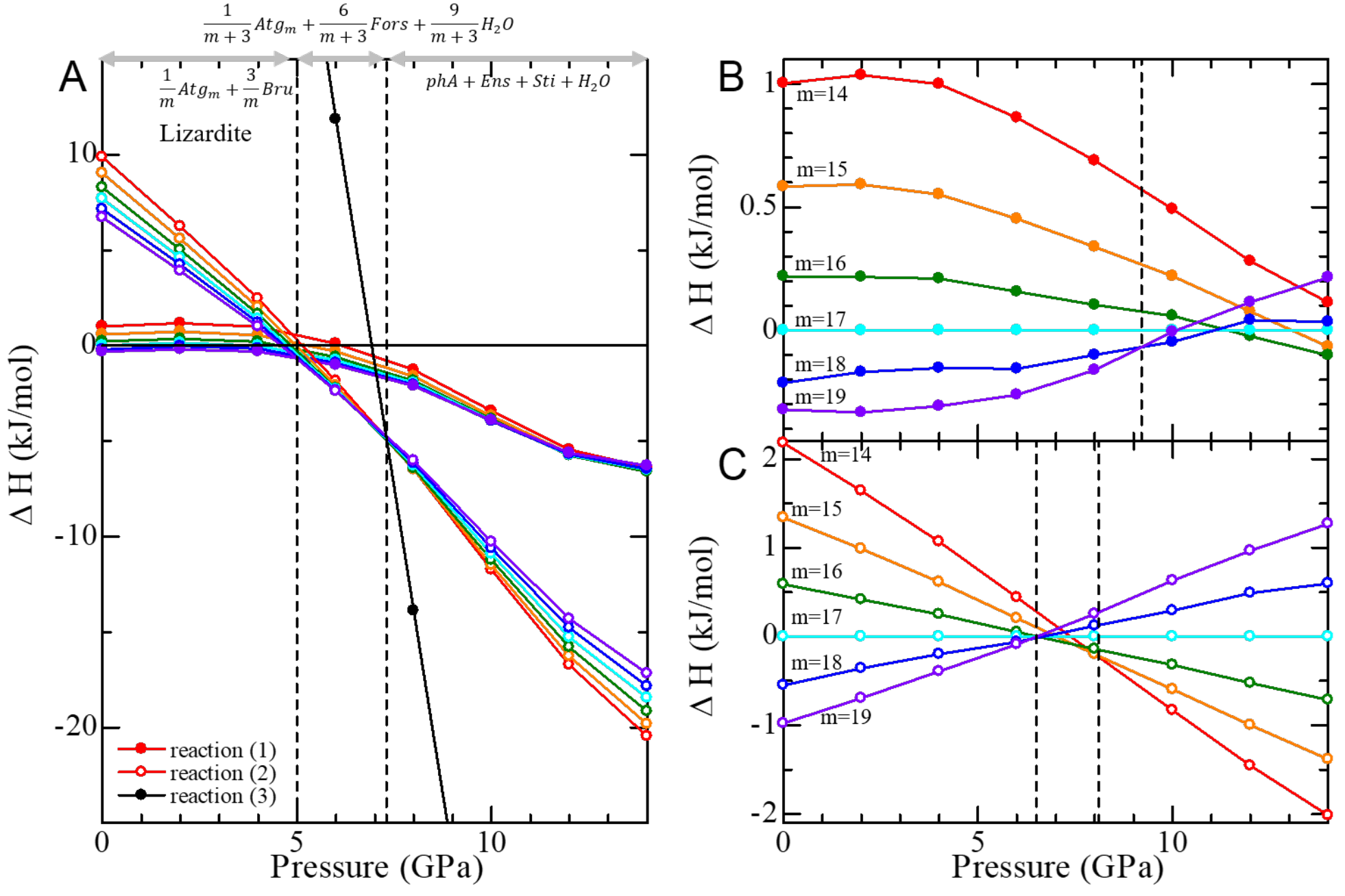
A
B
C
$\frac{1}{m+3}Atg_m + \frac{6}{m+3}Fors + \frac{9}{m+3}H_2O$
$\frac{1}{m}Atg_m + \frac{3}{m}Bru$
Lizardite
$phA + Ens + Sti + H_2O$
reaction (1)
reaction (2)
reaction (3)
Δ H (kJ/mol)
Pressure (GPa)
m=14
m=15
m=16
m=17
m=18
m=19